Lab on a Chip

Lymphangion-Chip: a microphysiological system which supports co-culture and bidirectional signaling of lymphatic endothelial and muscle cells

Journal:	*Lab on a Chip*
Manuscript ID	LC-ART-08-2021-000720.R2
Article Type:	Paper
Date Submitted by the Author:	22-Nov-2021
Complete List of Authors:	Selahi, Amirali; Texas A&M University College Station, Biomedical Engineering Fernando, Teshan; Texas A&M University College Station, Biomedical Engineering Chakraborty, Sanjukta; Texas A&M University System Health Science Center College of Medicine, Medical Physiology Muthuchamy, Mariappan; Texas A&M University System Health Science Center College of Medicine, Medical Physiology Zawieja, David; Texas A&M University Health Sciences Center, Department of Medical Physiology, Division of Lymphatic Biology Jain, Abhishek; Texas A&M University College Station, Biomedical Engineering; Texas A&M University System Health Science Center College of Medicine, Medical Physiology

Lymphangion-Chip: a microphysiological system which supports co-culture and bidirectional signaling of lymphatic endothelial and muscle cells

*Amirali Selahi[1], Teshan Fernando[1], Sanjukta Chakraborty[2], Mariappan Muthuchamy[2], David C. Zawieja[2], Abhishek Jain[1,2,3]**

[1]Department of Biomedical Engineering, College of Engineering, Texas A&M University, College Station, TX

[2]Department of Medical Physiology, College of Medicine, Texas A&M Health Science Center, Bryan, TX

[3]Department of Cardiovascular Sciences, Houston Methodist Academic Institute, Houston, TX

E-mail: a.jain@tamu.edu

*Address correspondence to this author:

Department of Biomedical Engineering
101 Bizzell Street
College Station, TX 77843
Phone 979-845-5532
Fax +979-845-4450

Keywords: organ-on-a-chip, experimental model, lymphangion, lymphatic endothelial cells, lymphatic muscle cells

Abstract:

The pathophysiology of several lymphatic diseases, such as lymphedema, depends on the function of lymphangions that drive lymph flow. Even though the signaling between two main cellular components of a lymphangion, endothelial cells (LECs) and muscle cells (LMCs), is responsible for crucial lymphatic functions, there are no *in vitro* models that have included both cell types. Here, a fabrication technique (Gravitational Lumen Patterning or GLP) is developed to create a Lymphangion-Chip. This organ-on-chip consists of co-culture of a monolayer of endothelial lumen surrounded by multiple and uniformly thick layers of muscle cells. The platform allows construction of a wide range of luminal diameters and muscular layer thicknesses, thus providing a toolbox to create variable anatomy. In this device, lymphatic muscle cells align circumferentially while endothelial cells aligned axially under flow, as only observed *in vivo* in the past. This system successfully characterizes the dynamics of cell size, density, growth, alignment, and intercellular gap due to co-culture and shear. Finally, exposure to pro-inflammatory cytokines reveals that the device could produce the regulation of endothelial barrier function through the lymphatic muscle cells. Therefore, this bioengineered platform is suitable for use in preclinical research of lymphatic and blood mechanobiology, inflammation, and translational outcomes.

1. Introduction

Lymphatics, as a one-way transport system, plays a crucial role in the human body, collecting interstitial fluid and proteins and returning them to blood circulation [1]. Besides, lymphatic vessels carry the significant tasks of immune cell trafficking and lipid absorption [1]. Despite their vital role in maintaining body homeostasis and initiating numerous conditions such as cancer metastasis, lymphatic vascular physiology remains understudied relative to the blood vasculature [2-4]. While several *in vivo* and *ex vivo* animal models exist and have contributed to some significant discoveries in the field [5, 6], they can lack predictive power. Also, there are relatively few multicellular *in vitro* models of lymphatic vessels that include relevant cell-cell interactions. Microfluidic models of blood and lymphatic vessels are emerging, which provides an enormous opportunity to fill this gap. Still, the ones that exist mostly focus on characterizing lymphatic endothelial permeability [7-11], tumor-lymphatic interactions [12-16], and lymphangiogenesis [17, 18], and none of these devices have included lymphatic muscle cells yet. A lymphangion is the functional unit of lymphatics, containing two major cell components: lymphatic muscle cells (LMCs) and lymphatic endothelial cells (LECs) [19]. LMCs are crucial in lymphatics, as they lead to efficient drainage, luminal flow, and pressure regulation [20]. Dysfunction of the lymphatic muscle may contribute to the development of pathologies such as lymphedema, for which there is no available cure [21, 22]. Conversely, the secretion of mediators from LECs in various shear stress conditions has been shown to regulate muscle tissue [23]. However, existing tools lack the proper cylindrical microenvironment for cells to experience *in vivo* physiological stress and strain conditions [7, 15, 16]. For example, the morphology and alignment of LMCs play a significant role in their function and molecular response [24]. Based on *in vivo* observations, LMCs can be found packed in a relatively thin muscle layer while maintaining a uniform density around endothelium at each vessel's cross-section [25-27]. However, the current fabrication techniques to obtain 3D vasculature models result in either asymmetrical [28-30] or relatively thick and non-physiological ECM layer [12, 31] surrounding the lumen. Similarly, LEC-LMC

crosstalk is known to play a significant role in lymphatic function and this LEC-LMC signaling can be due to mechanical or inflammatory cues [32, 33]. Although the effect of physical forces on LECs alignment and LMCs remodeling have been studied individually [24, 34], there remains a need to study the LEC-LMC signaling under mechanical and inflammatory conditions in a representative model.

Here, we engineered the first 3D cylindrical lymphangion-on-chip (Lymphangion-Chip) consisting of the co-culture of LECs and LMCs within an extracellular matrix for several days under fluid shear (**Figure 1**). With a fabrication technique specifically developed to wrap LMCs uniformly around the LECs, we showed that both LMCs and LECs maintain their essential phenotype, growth and subendothelial characteristics, and morphological alignment, as either seen or expected *in vivo*. We then characterized the sensitivity of co-cultured LECs and LMCs due to shear and inflammatory cues. Overall, the data suggest that the Lymphangion-Chip will serve as an experimental model for preclinical lymphatic (and blood) vascular research and pharmacological testing.

2. Results

2.1. Design and engineering of the Lymphangion-Chip

We were inspired to create Lymphangion-Chip as a platform technology offering control over geometry, mechanical properties, and fluid dynamics relevant to the diversity of lymphangions *in vivo*.

Importantly, our aim was to create a cylindrical/elliptical microfluidic organ-chip consisting of a monoculture of LECs surrounded by multiple layers of uniformly thick LMCs embedded inside collagen hydrogel as an initial supporting ECM. While several lumen forming techniques exist in literature [28, 31, 35-43], there are relatively very few that can be easily be made cylindrical or elliptical and can also support culture of the muscle cells in an *in vivo* like morphology. In particular, viscous finger patterning method has now been adopted several times to make microfluidic endothelialized lumens [28, 44, 45], but in co-culture settings, this method has not demonstrated a uniform distribution of wrapped muscle cells around the endothelium. This technique is believed to rely primarily on viscous fingering (also known as

Saffman-Taylor instability) that is a fluid dynamics phenomenon in which a less viscous fluid (cell medium) flows through and displaces a more viscous liquid (liquid collagen), creating finger-shaped structures. We hypothesized that in this technique, convective fluid dynamics characteristics - fluid pressure head across the inlet and outlet of the microfluidic channel and gravity – also determine the size and position of the lumens than solely liquid displacement due to the differences in two fluids viscosities.

To test this hypothesis, we perfused an LMC-hydrogel mixture into the device by keeping an inlet reservoir and producing vacuum inside the channel using a syringe connected to outlet, either when the device is placed horizontally on the incubator rack (classical viscous fingering method) or when it is rotated 90° to align the channel's axis with gravitational direction (Gravitational Lumen Patterning or GLP). While keeping the device in this position, less viscous fluid (cell medium) displaced high viscous fluid (collagen-LMC mixture) and formed a lumen (**Figure 2A**). When GLP method was adopted, the thickness of the ECM was relatively conserved in different angular positions around the inner hollow cavity, as observed by doping the matrix with fluorescent beads (**Figure 2B, C**) or by directly visualizing the LMCs within the matrix (**Figure 2D**). This relatively uniform distribution was absent when we adopted the classical viscous fingering technique. We suspect that due to the buoyancy effect, the higher density fluid (collagen) tends to displace the lower density liquid (cell medium) and push it up toward the top of the channel, thus resulting in a variably thick ECM around the lumen. However, by keeping devices vertically and hence, aligning the gravitational force in the vessel's axial direction, we prevented this transverse effect of buoyant force and established a 3D lumen with a nearly symmetrical cross-section.

Then, we used GLP technique to build Lymphangion-Chips of variable sizes and ECM thicknesses. By changing the hydrostatic pressure at the chip inlet (140 to 340 Pa) while performing GLP, we could modulate the lumen diameter from a range of 400 μm to 800 μm (**Figure 3A, B**). Also, since collagen

concentration is directly proportional to its viscosity and hydraulic resistance, we found that increasing the collagen concentration from 3 to 5 mg/ml (~60%) during GLP resulted in a 30% lumen size reduction (**Figure 3C, D**). We also altered the outer lumen diameter (i.e., the vessel's thickness) by manufacturing molds with 600, 400, and 200 μm channel widths and confirmed that lumen formation using GLP was successful in this range as well (**Figure 3E**). Taken together, these results show that mechanical factors, such as hydrostatic pressure, microchannel size, and gravitational effect, as well as our supporting biomaterial - collagen concentration - can be varied to create hollow lumens of a wide range of sizes, thicknesses, and interstitial mechanical properties relevant to lymphatic vessels.

2.2 Reconstitution of lymphatic endothelial and muscle tissue in Lymphangion-Chip

Since the endothelial and muscle cells are the two main tissue components of a lymphatic vessel [46], we set out to confirm if we can co-culture these two lymphatic cell types in our GLP microfluidic constructs using just one cell culture media formulation. In the beginning, we seeded only LECs on the luminal side of the chip and found that LECs formed a monolayer of confluent endothelial cells with properly formed cell-cell junctions in nearly two days. Using cell specific culture medium, LECs stayed confluent even after five days, and barrier integrity was maintained (**Figure 4A**). In the next experiment, LMCs alone were mixed with collagen and perfused within the device. After five days of monoculture using the medium specified for this cell, we found that LMCs formed multilayers of oval-shaped structures embedded inside the collagen matrix, similar to observed *in vivo* morphology [25, 26]. We evaluated distribution and proliferation and confirmed the presence of LMCs all over the lumen (**Figure 4B**). Next, to identify the standard cell culture condition for a successful co-culture, we investigated the effect of environmental CO_2 percentage and cell medium combination on LMC and LEC growth, respectively. We observed that even though LECs reached full confluency in all combinations of LEC:LMC medium, CO_2 of 5% and LEC:LMC of 1:0 and 3:1 resulted in 100% cell coverage in less than 60 hours. In contrast, LMCs were more sensitive to LEC:LMC medium for which only LEC:LMC of 1:0 and 1:3

resulted in 100% confluency (**Figure 4C, D**). Based on these datasets, we identified that CO_2 of 5% and LEC:LMC medium ratio of 1:3 may be suitable for the co-culture. Using the derived formulation, a mixture of LMCs and collagen was perfused in the device, followed by lumen formation via GLP technique. After one day, LECs were seeded through the lumen on the collagen face and were kept in the incubator. Confocal fluorescence microscopic analysis revealed that a confluent layer of endothelium surrounded by multiple layers of muscle cells was formed on-chip (**Figure 4E**). In co-cultured devices, the average lumen inner diameter and muscle layer thickness is measured as nearly 750 μm and 150 μm, respectively. These images provide the first evidence of a successful lymphatic vessel-on-chip consisting of both LECs and LMCs cultured together using a common medium formulation.

To assess the physiological relevance of the LEC and LMC interface, we examined the on-chip endothelium and muscle layer gap as well as cell growth in co-culture versus monoculture conditions. The gap between LEC and LMC layers stayed nearly uniform under LMC monoculture, but it reduced steadily over time and reached nearly 5 μm in 4 days after LEC-LMC co-culture (**Figure 5A-C**). Thus, LMCs respond and migrate toward LECs resulting in a time-dependent decrease in the subendothelial gap that is consistent with prior *in vivo* and *in vitro* observations for vascular cells [47]. Correspondingly, our observation of on-chip cell culture over four days post-seeding revealed that LEC density increased over time and reached confluency within three days after culture (**Figure 5D**). This observation was independent of the presence of LMCs, however, when LECs were co-cultured with LMCs, their cell density was significantly less compared to monoculture condition. The increase in the LEC density positively correlated with less average cell size over time due to the squeezing of cells within the endothelium layer (**Figure 5E, F**). Meanwhile, the LMC density also increased in the first two days and plateaued after, with no particularly significant difference between monoculture vs. co-culture with LECs at the end of 5 days (**Figure 5G, H**). These on-chip LEC and LMC growth dynamics that we

characterized and validated for the lymphatics suggest an active presence of LEC and LMC signaling that were previously observed in other *in vitro* vascular models of only blood cells [48-50].

2.3 Assessment of lymphatic cells due to physical cues within Lymphangion-Chip

The physiological arrangement of lymphatic cells *in vivo* is such that a high percentage of muscle and endothelial cells align perpendicular and parallel to the vessel's axial direction, respectively [25, 51-54]. We speculated that this cell alignment – LMCs perpendicular to axially aligned LECs – will be facilitated by the co-culture of LECs with LMCs. To test this, we compared the lymphatic cell orientation in co-culture versus monoculture within the chip. We prepared three sets of devices containing: only LMCs, only LECs, and LMC-LEC co-culture. After five days of monoculture, we found that LMCs aligned mostly axially in all lumen sections (sides, top, and bottom). However, co-cultured with LECs, most LMCs were circumferentially oriented (i.e., perpendicular to the axial vessel direction) (**Figure 6A**). Further, when we exposed the LEC-LMC co-culture to a typical physiological shear (1 dyne/cm^2) [55], we found a significantly more axial alignment of LEC and circumferential alignment of LMC, relative to static culture conditions (**Figure S1**). The LEC alignment in the flow direction within Lymphangion-Chip matches the previous *in vitro* studies for endothelial cells [54, 56-58]. Interestingly, when we applied an intermediate shear (0.1 dyne/cm^2) representative of the lymphedema condition in which the lymphatic system's blockage prevents efficient lymph drainage [59, 60], we observed a relatively poor axial alignment of LECs and circumferential alignment of LMCs. Also, regardless of the shear, co-culturing muscle cells with endothelial cells always produced a relatively more axial orientation of LECs and circumferential orientation of LMCs, strengthening the device's capability to include active signaling between the two cell types (**Figure 6B-D**).

2.4 Evaluation of lymphatic endothelial barrier function due to inflammatory cues within Lymphangion-Chip

Several studies support the role of inflammatory cytokines, including TNF-α, in endothelial dysfunction and increased permeability[61]. TNF-α is known to decrease lymphatic contractility [62] and disrupt the lymphatic endothelial barrier function [63]. Since the *in vitro* effect of TNF-α on LEC-LMC co-culture has not been characterized before, we finally set out to illustrate the power of Lymphangion-Chip as a tool to systematically investigate how LMCs could regulate LECs function under the influence of inflammatory signals. First, to characterize the lymphatic endothelial permeability, we measured the diffusion of fluorescein isothiocyanate (FITC)-Dextran [64], and found that dextran may diffuse through lymphatic endothelial cells as a function of its molecular weight (**Figure 7A, B**). The vessel permeability for 4 kDa molecules (3×10^{-5} cm/s) was significantly larger than the same for 20 and 70 kDa conjugates ($<5\times10^{-6}$ cm/s) (**Figure 7C**). These results confirm that Lymphangion-Chip's endothelium is leakier for small molecules compared to larger molecules that possess the size of albumin (~68 kDa), supported by observations made in animal models [65]. Next, when we exposed the Lymphangion-Chip to TNF-α either when LECs and LMCs were cultured alone or together, we found a significant increase in permeability relative to our untreated controls. However, when LMCs were co-cultured with LECs, we discovered that the lymphatic endothelial barrier function was relatively conserved, suggesting its influence in maintaining tissue homeostasis (**Figure 7D**). The specific signaling pathways involved in LMC-induced recovery post-inflammation is an intriguing topic to study with our platform in the future.

3. Discussion

The endothelial and muscle cells are two key cell types that generate and regulate lymph flow in lymphatics and set the vessel's response to mechanical stimulation and inflammation [20, 66, 67]. The normal interactions between these two cell types are important for the homeostasis of the lymphatic transport, and any aberrant interaction between them may lead to loss of junction integrity and flow [68]. But, this LEC-LMC signaling is not fully characterized in experimental models, and the relatively few *in vitro* studies

that exist have attempted to unveil the effects of mechanical forces only on LECs [69]. Several multicellular vascular organ-on-chip models have now been published and are currently being deployed in preclinical research and pharmaceutical discoveries [70], including designs to co-culture endo/epithelial and smooth muscle cells in rectangular multichannels [71, 72]. Even though these models demonstrate vascular EC-SMC co-culture and arterial function [71], the muscle layer is not wrapped circumferentially around endothelium as seen *in vivo*. Notably, there is currently no design to co-culture and study cell signaling between lymphatic endothelial and mural cells. Importantly, no studies have included the lymphatic muscle cells in their *in vitro* studies or culture them appropriately with the endothelium. To address this gap and enable prolonged LECs-LMCs co-culture in a physiologically relevant environment, we created a 3D cylindrical Lymphangion-Chip through gravitational viscous finger patterning or GLP that harnesses the control of the buoyant effect and pressure difference across the channel not done before in prior designs. Our results show that this platform affords flexibility in determining the physical and geometrical parameters of a lymphangion. By fabricating Lymphangion-Chip with GLP method, we offer a toolbox to alter lumen inner and outer diameter as well as muscle tissue stiffness and thickness in a robust and physiologically-relevant manner [19, 53, 73, 74]. Therefore, this engineered tunable platform may also guide future studies beyond what we present here and can be leveraged in studying other types of vascular tissues.

Our observation of a time-dependent decrease in the subendothelial gap strongly suggests proactive LEC-LMC signaling as LECs and LMCs grow and proliferate within the device. The growth factors released by endothelial cells, such as polypeptide platelet-derived growth factor-B (PDGF-B) [47, 75], may produce a concentration gradient around the endothelial layer, promoting the proliferation and migration of LMCs toward the endothelium layer, via their surface receptors, such as tyrosine kinase receptor PDGFR-β [75, 76]. Future studies may allow such a hypothesis to be effectively tested with our platform. Also, proliferative smooth muscle cells are known to inhibit endothelial cell proliferation [48, 77]. Within Lymphangion-Chip, we saw a similar growth pattern, and the LECs growth rate was inhibited in co-culture conditions. The

mechanisms that regulate such lymphatic endothelial-muscle cell crosstalk are beyond the scope of this work; however, this platform can be used for such studies without a significant need for animal models. Since our approach produces a symmetrical and cylindrical lumen surrounded by a matrix, we could co-culture LECs and LMCs to align in the axial and circumferential direction, respectively, as frequently observed *in vivo*. Our device further demonstrated a robust sensitivity of this relative alignment of the two cells with respect to the presence or absence of co-culture and mechanical forces (shear stress), thus suggesting that LECs and LMCs are biologically and functionally active within the chip.

The lymphatic vasculature is essential in modulating the inflammatory response by altering interstitial fluid extravasation and drainage. During inflammation, the lymphatic vessel experiences a significant enlargement in inflamed tissue leading to an elevation in vessel leakiness and thus losing its full functionality [78]. Studying LEC monolayer integrity has shown that endothelium permeability increases in response to inflammatory stimuli [63]. However, the effect of LMCs in cytokine-induced hyperpermeability of the endothelium is largely unknown. Lymphangion-Chip revealed the possibility of the contribution of LMCs in partial recovery of endothelial barrier function after exposure to TNF-α. Although our absolute permeability measurements are typically higher than those quantified for *ex vivo* animal models, likely due to the difference in methodology, cell type etc [79, 80], the trends we have obtained are fairly consistent with other reports of *in vitro* lymphatic vascular models [11]. While detailed signaling analysis of LMCs in barrier function recovery is beyond the scope of this study, we expect that the Lymphangion-Chip can be used to assess the clinical relevance and consequences of such LEC-LMC crosstalk in subsequent studies.

Our Lymphangion-Chip has not reached its full potential. For example, there is an opportunity to include pericytes in the model. Also, even though we introduced shear uniformly, in the collecting lymphatics, flow and pressure are uniquely pulsatile in nature [51]. It may be critical to introduce such flow profiles for some future studies that investigate lymphatic mechanobiology. Also, lymphatic vessels exhibit phasic and tonic contractility in most murine models, if not all [81], but we did not focus on in this work. Although

pacemaker cells are believed to initiate lymphatics phasic contractions, prior studies suggest that external stimulation (for example, by including electrical energy) may also be needed to initiate such contractile activity ***in vitro*** [82, 83]. Some prior literature also suggests that these cells may partially maintain their tonic contractions in the 3D matrix [84]. Thus, Lymphangion-Chip can potentially be used to characterize muscle tonic contractile behavior that can be more directly characterized in future studies. Finally, LMCs and LECs in this project are derived from rat mesenteric vessels and human dermal tissue, respectively. This is a limitation because human LMCs are not commercially available.

4. Conclusion

In summary, this organ-chip technology allows us to include essential lymphatic vascular components in a tunable 3D physiological environment. We can easily dissect and control several variables such as flow, geometry, chemical cues, etc., that impact LECs and LMCs in a way that may potentially result in a translational impact. This platform can be immediately combined with molecular and gene analysis tools to provide more precise insight into the regulatory signaling mechanisms of lymphatic vascular physiology/pathophysiology and drug treatments. Finally, the platform can also be applied in blood vascular models

5. Experimental Section/Methods

5.1 Lymphangion-Chip design and fabrication

The microfluidic channels of the platform were designed using SolidWorks (900 μm wide, 900 μm high, 5 mm long, 1.5 mm diameter inlet reservoir, 2 mm diameter outlet reservoir) and were subsequently 3D printed on VeroWhite Resin using an Eden350 setup to make the mold. Then, the microfluidic devices were fabricated by soft lithography of polydimethylsiloxane (PDMS, Dow Corning). Briefly, base and cross-linker were mixed at a 10:1 ratio, and then the mold was filled with PDMS mixture and cured at 80° C for 2 hours. Later, the PDMS slab was removed from the master mold, and the inlets and outlets were

punched with a 1-mm biopsy punch (Ted Pella). Finally, the PDMS slabs containing the channel features were plasma bonded to a PDMS-coated glass slide using a 100 Watts plasma cleaner (Thierry Zepto, Diener Electronics), and devices were kept at 80° C for 30 minutes to enhance the binding. The detailed protocol is published elsewhere [85].

5.2 Device pretreatment and gravitational lumen patterning

The devices were pretreated before hydrogel perfusion to enhance the collagen-PDMS bonding strength using a previously described protocol [86]. In brief, the devices were plasma treated and silanized immediately by filling with 10% v/v silane ((3-Aminopropyl)trimethoxysilane, Sigma-Aldrich) in ethanol. After 15 minutes of incubation at room temperature, the channels were washed extensively with ethanol and kept in an 80° oven for 2 hours to dry. Then, the devices were filled with 2.5% v/v glutaraldehyde (Sigma-Aldrich) and were kept at room temperature for 15 minutes. Finally, the microfluidic devices were washed multiple times with ethanol and kept in the 80° oven for 2 hours (**Figure S2A**).

The devices were first degassed in a vacuum chamber for two hours and then filled with ice-cold high concentration hydrogel-LMCs mixture (see next section) using vacuum produced by connecting syringes to the outlets (**Figure S2B**). Then, the inlet tips were removed and the devices were rotated 90° to align the microfluidic channels parallel to gravity direction (vertical position). Later while the devices were kept vertically, additional curved tips filled with 50 µl of ice-cold cell medium were released at the inlets. In the vertical position, the curved tips were both facing upward in a manner to share a horizontal line to force stop cell medium flow after lumen formation (**Figure S2B**). After observing the cell medium flow from the inlets to the outlets, the devices were placed in a 37° incubator while their position was fixed either vertically using a clips. The tips were removed gently after 7 minutes to avoid collagen-plastic tip adhesion, and the devices were turned back again to horizontal position. The tips were replaced with cell medium droplets to prevent air bubble formation in devices inlets and outlets.

After 30 minutes of incubation, the devices were removed from the incubator, and fresh syringe tips were added gently to the inlets and outlets (**Figure S2C**). At this point, the collagen was already polymerized, and the 3D lumen could be observed using a phase-contrast microscope. Next, the devices were washed substantially but gently with the cell medium. To achieve this, each time, only 50 µl of warm cell medium was added to the inlet tips while the excessive solution was removed from the outlet tips. This process was repeated multiple times resulting in the passive pumping of the cell medium within the lumen to wash away all the chemical solution remained within ECM (**Figure S2D**).

5.3 Lymphatic cell culture

We employed a previously published technique to isolate endothelial cells and muscle cells from rat mesenteric lymphatic vessel [87-89]. In summary, after isolation of rat mesenteric collecting lymphatics, the vessel was cleaned and incubated on a gelatin-coated plastic culture dish. High-glucose Dulbecco's modified Eagle's medium supplemented with 20% FBS, 2mM sodium pyruvate, 2mM L-glutamine, and antibiotics was added to the dish to promote the growth of LMCs. Then, the vessel was removed after migration of the muscle cells out of the vessel's cut sections (after 3-4 days). In this step, LMCs can be recognized by their morphology and also by negative uptake of fluorescent acetylated-LDL which is taken up specifically by endothelial cells via the "scavenger cell pathway" of LDL metabolism [90]. If some colonies of LECs were observed in culture, it was eliminated physically with a rubber policeman or by laser ablation using a UV laser microscope. Finally, LMCs were kept to grow further and then were trypsinized and passaged after 7-10 days. The used protocols for rat cells isolation were approved by the Texas A&M University Laboratory Animal Care Committee (IACUC 2019-0284). The human dermal LECs were purchased commercially (Promocell). All cells were cultured separately in standard cell culture flasks featuring vacuum-gas plasma tissue culture treatment (ThermoFisher Scientific) and were passaged after reaching 90% cell confluency (passage 4-7). LECs were maintained with 99% v/v Endothelial Cell Growth Medium MV2 (full supplemental kit, PromoCell) and 1% v/v antibiotic

cocktail (Gibco) in a humidified 37° and 5% CO_2 incubator, while LMCs were kept in 89% v/v DMEM/F-12 (Gibco), 10% v/v FBS (Gibco) and 1% v/v Antibiotic cocktail in a 10% CO_2 incubator. To achieve on-chip 3D cell culture, LMCs were first trypsinized and resuspended in 33 µl DMEM/F12 and then extensively mixed with a solution of 110 µl high concentration rat tail type I collagen (9 mg/ml, Corning), 40 µl HEPES (1M, Gibco), 14 µl Sodium Bicarbonate (NaHCO3, 1M, ThermoFisher Scientific), and 3 µl Sodium Hydroxide (NaOH, 1M, ThermoFisher Scientific) with the final concentration of 5×10^6 cells/ml. The cell-gel mixture was then used in GILP process to form the 3D lumen (described previously). The devices were kept for one day before seeding LECs, while the LMC medium was exchanged twice a day. Next, LECs were seeded using the previously described method with modifications [91]. In summary, endothelial cells were trypsinized and added to the co-culture medium (1:3 LEC:LMC medium, see RESULTS) with a final concentration of 2.5×10^6 cells/ml. Then, the devices were filled with the cell suspension and were incubated in a 5% CO_2 incubator for 40 minutes for cells to adhere fully to collagen. After flushing unadhered cells using the fresh medium, devices were turned upside down, and this same process was repeated four times for each side of the lumen (Supplementary Fig. 3D). The co-culture medium was exchanged twice a day, each 15 minutes, for devices under no-flow conditions. For flow experiments, devices were connected to a programmable syringe pump (Harvard) to apply a constant and continuous flow rate that resulted in the average wall shear stress measured in rat mesenteric lymphatic vessel (~1 dyne/cm^2) [55, 92]. To model lymphedema-like conditions (i.e., inadequate lymph drainage and inflammation), the flow rate was reduced by 10-fold, resulting in ~0.1 dyne/cm^2 wall shear stress.

5.4 Immunohistochemistry

Immunohistochemistry of Lymphangion-Chip devices was performed with standard fixation (4% paraformaldehyde, Sigma), permeabilization (0.5% Triton X-100, Sigma), and blocking (10% Bovine Serum Albumin, ThermoFisher Scientific) methods. Fixed devices were later incubated with mouse or

rabbit primary antibodies, including α-smooth muscle actin (α-SMA, eBioscience), vascular endothelial-cadherin (VE-cadherin, Invitrogen), or Lymphatic vessel endothelial hyaluronan receptor 1 (LYVE1, Invitrogen) followed by secondary anti-mouse or anti-rabbit fluorescent antibodies (Invitrogen). Finally, cell nuclei were stained with Hoechst 33258 (Invitrogen).

5.5 Cell functional assessment

To evaluate on-plate and on-chip cell density and confluency, we used the non-invasive and non-destructive method described before [93]. Quantification of cell alignment was performed using OrientationJ, a Fiji software plug-in for directional image analysis based on evaluating gradient structure tensors [94, 95]. OrientationJ software code was used to characterize the orientation and isotropic properties of a region of interest in an image, based on the evaluation of the structure tensor in a local neighborhood [96]. To employ this method, LECs and LMCs were fixed and stained with Hoechst and α-SMA, respectively [34]. Then, z-stack confocal images were taken of the devices to capture all cells within the vessels. All images were bandpass filtered using high- and low- frequency cut-offs at 2 and 20 pixels. Finally, images were post-processed to obtain the tensor containing angle θ of cells alignment with respect to the axial direction by analyzing nuclei and actin orientation. Finally, the distribution of cell alignment was plotted on a polar histogram. In order to measure the gap size between endothelium and muscle tissue, orthogonal views of the 3D confocal images of devices were plotted and then the average distance between the nearest LMCs to endothelium layer for the whole device were measured and plotted in each time-point.

5.6 Inflammatory cytokine treatment

The cytokine treatment started after four days of endothelial cell culture to ensure the formation of a confluent intact endothelium layer. After removing the cell medium and replacing it with the phenol-free experimental medium, we waited for 2 hours for cells to stabilize. Then, 50 µl medium containing TNF-α (10 ng/ml, recombinant from E. coli, Sigma) was added to the devices [63, 97, 98]. After 2 hours, 50 µl of

cell medium mixed with FITC labeled BSA was added to the vessels, and fluorescent images were taken immediately and after 30 minutes.

5.7 Endothelial permeability measurement

To measure vessel permeability, 50 µl of 1 µM working concentration of Dextran solution (Texas Red dextran, 4 kDa, 20 kDa, and 70 kDa, ThermoFisher Scientific) in the phenol-red free medium was added to the device inlet while aspirating the experimental medium of the device outlet. Therefore, the fluid within the inlet and outlet reservoirs reached the same elevation quickly to minimize flow and pressure increase inside the vessel. The solute transport inside the vessel was then measured immediately and after 30 minutes of diffusion. We plotted the fluorescence intensity on three vertical lines along the vessel length. The vessel-on-chip permeability coefficient was calculated using Eq. 1 [99]:

$$P = \left(\frac{1}{I_0}\right)\left(\frac{I_f - I_0}{t_f - t_0}\right)\left(\frac{D}{4}\right) \qquad \text{Eq. 1}$$

where I_0 and I_f are the total florescent intensities outside the vessel at 0 and 30 minutes, respectively. I_0 and I_f were calculated by summing up the area under the curve for fluorescent intensities from the LECs monolayer to the channel wall. t_0 and t_f are the initial and final timepoints, and D is the vessel diameter.

5.8 Imaging and microscopy

Standard fluorescent and phase-contrast images were acquired using Zeiss Axio Observer Z1 inverted setup (LD Plan Neofluar, 10X, NA 0.4) and Zeiss Axio Vert.A1 (DIC, Axiocam 503, 20X, Zeiss), respectively. Images were analysed and processed with ZEN 2.3 lite software (Zeiss). Z-stack and stitched confocal images were obtained with an Olympus FV1000 microscope. Live-cell images were captured with a CytoSMART 2 system.

5.9 Statistical analysis

Data and error bars are represented as the mean and standard error of the mean (SEM), respectively. Statistical analysis was performed using GraphPad Prism v7 (GraphPad Software Inc.). The comparison

between data groups was carried out using the student t-test, and a P value of less than 0.05 was considered statistically significant.

6. Acknowledgements

We thank Dr. S. Vitha at the Microscopy and Imaging Center at Texas A&M University for assisting with confocal imaging. Research reported in this publication was supported by the NIBIB R21EB025945, NSF CAREER Award number 1944322, Texas A&M Engineering; and President's Excellence in Research Funding Award of Texas A&M University to A.J.

7. Author contributions

A.S. performed the microfluidics experiments. A.S. and A.J. analysed results, made the figures, and wrote the paper with feedback from all authors; T.F. performed the experiments to find the coculture conditions for LECs and LMCs used in this study; S.C., M.M and D.C.Z. isolated and characterized the lymphatic muscle cells used in this study, and M.M and D.C.Z. also contributed to data analysis.

8. Conflict of interest

The authors declare no conflict of interest.

FIGURE LEGENDS

Figure 1 Lymphangion-Chip: Microfluidic model of a lymphangion. (**A**) Illustration of the human lymphatic vessel consisting a lymphangion which is the unit between the two adjacent valves and (**B**) an engineering drawing of Lymphangion-Chip with co-cultures of lymphatic endothelial cells (LECs) and lymphatic muscle cells (LMCs) that is leveraged to analyze the responses to flow and inflammatory cues. (**C**) A representative confocal image set of on-chip LMCs (green: F-actin) and LECs (green: VE-Cadherin) in co-culture condition. scale bar: 50 μm

Figure 2 Gravitational Lumen Patterning (GLP) technique to fabricate Lymphangion-Chip. (**A**) The LMC-matrix mixture was perfused into the device by producing vacuum using a syringe connected to the outlet. Then, the devices were rotated 90° (vertical position) so that the microfluidic channel aligned parallel to the direction of gravity. While keeping the device in vertical position, a curved tip filled with LMC medium were added to the inlet while rotating the outlet tip so that both tips share a horizontal plane (equal level) for the cell medium not to flow out of the device. In this case, the less viscous fluid (cell medium) would wash away the high viscous fluid (hydrogel) and form 3D symmetrical lumen. (**B**) The fabricated device containing the lumen formed by GLP (**C)** Side and cross-section views of the 3D lumen (green: fluorescent beads adhered to the collagen surface demonstrating the lumen boundary). (**D**) Effect of gravity on lumen symmetry when the device axis is perpendicular or parallel to gravity direction. Scale bars: 200 μm; n = 3 for the experimen

Figure 3 Engineering and tuning of Lymphangion-Chip. (**A**) Graph and (**B**) representative images of engineering the lumen inner diameter and the muscle tissue thickness by setting hydrostatic pressure and (**C, D**) collagen concentration. (**E**) Engineering the outer vessel diameter by running GLP method in chips with various channel widths (200 – 600 μm) (Mixture of green fluorescent beads with cell medium specifies the lumen). All scale bars: 200 μm; *p < 0.05, **p < 0.005, ****p < 0.0001; n = 3-5 for all the experiments.

Figure 4 Reconstitution of lymphatic endothelial and muscle tissue in Lymphangion-Chip. (**A**) A confluent monolayer of LECs (top right: Lyve-1) is formed on top of the collagen. The phase-contrast image (bottom right) and VE-cadherin staining (bottom left) demonstrate the tight LECs junctions after vessel formation. (**B**) LMCs proliferation in multilayers in the 3D collagen matrix (α-smooth muscle actin: green, nuclei: red). (**C**) LECs and (**D**) LMCs growth study in various ratios of LEC:LMC medium and CO_2 % by measuring the cell confluency over time. LEC:LMC medium of 1:3 along with 5% CO_2 results in 100% cell confluency after nearly 60 hours of cell culture. (**E**) Confocal 3D fluorescence images of Lymphangion-Chip in the optimum co-culture conditions demonstrating a confluent layer of endothelium surrounded by multiple layers of muscle cells (green: α- smooth muscle actin as LMC marker, red: Lyve-1 as LEC marker). All scale bars: 100 μm; n = 5 for all experiments.

Figure 5: Assessment of lymphatic endothelial and muscle cells within Lymphangion-Chip. (**A**) Confocal cross-sectional image showing LECs (red) surrounded by LMCs (green); Scale bar: 200 μm. (**B**) The average gap distance between endothelium and muscle layers over 96 hours after cell culture, shown graphically, and (**C**) via representative images of LECs (red) and LMCs (green); Scale bar: 20 μm. (**D**) LMCs density and (**E**) size vs. time either in monoculture (solid line) or co-culture with LMCs (dotted line). (**F**) Representative images of LECs showing an increase in cell density and decrease in cell size when cultured on-chip; Scale bar: 50 μm. (**G**) Graph and (**H**) representative images of LMCs (green) density in the 3D ECM in monoculture versus co-culture; Scale bar: 50 μm; *p < 0.05, **p < 0.005; n = 5-7 for all experiments.

Figure 6: Assessment of lymphatic cells due to physical cues within Lymphangion-Chip. (**A**) LMC alignment in monoculture versus LEC-LMC co-culture conditions. LMCs (green) tend to orient mostly axially in monoculture. In contrast, co-cultured with LECs (red), LMCs align circumferentially which is closer to *in vivo* condition (green: α-smooth muscle actin; red: Lyve-1). (**B**) The polar histograms of LEC and LMC alignment in three conditions: no flow, low shear, and normal shear. LMCs orient more circumferentially in normal shear conditions (i.e., higher shear rate) while LECs orient in the flow direction. Heatmaps of (**C)** LEC and (**D**) LMC mean orientation angle in monoculture and co-culture while being exposed to no flow, low shear, or normal shear conditions. All scale bars: 200 μm; n = 5 for all experiments.

Figure 7 Evaluation of lymphatic endothelial barrier function due to inflammatory cues within Lymphangion-Chip. (**A**) Representative fluorescent images of FITC-dextran diffusion through LEC monolayer. Two sets of images are captured from the vessel in 0 and 30 minutes after perfusing the FITC-dextran conjugates, shown in the left and right panels, respectively (green: fluorescent conjugates). (**B**) Normalized fluorescent intensity plot for different FITC-

conjugate sizes within Lymphangion-Chip. We plotted normalized Gaussian curves for 0 and 30 minutes after perfusion of three sizes of FITC-conjugates. (**C**) Measured permeability using the area under the curve for Lymphangion-Chip. Smaller FITC-dextran conjugates perfuse easier through endothelial cell gaps, thus, result in larger permeability values. (**D**) Permeability for Lymphangion-Chip made of only LECs and LEC-LMC co-culture before and after exposure to TNF-α as an inflammatory cytokine. TNF-α enhances the vessel permeability in both conditions leading to larger values for permeability. When co-cultured with LECs, LMCs help in partial recovery of endothelium permeability after inflammatory cytokine treatment. Scale bar: 200 μm; *$p < 0.05$, **$p < 0.005$, ***$p < 0.001$, ****$p < 0.0001$; $n = 5$ for all experiments.

References

1. Swartz, M. A., The physiology of the lymphatic system. *Advanced drug delivery reviews* **2001,** *50* (1-2), 3-20.
2. Rockson, S. G., Lymphedema. *The American journal of medicine* **2001,** *110* (4), 288-295.
3. Stacker, S. A.; Williams, S. P.; Karnezis, T.; Shayan, R.; Fox, S. B.; Achen, M. G., Lymphangiogenesis and lymphatic vessel remodelling in cancer. *Nature Reviews Cancer* **2014,** *14* (3), 159-172.
4. Paduch, R., The role of lymphangiogenesis and angiogenesis in tumor metastasis. *Cellular Oncology* **2016,** *39* (5), 397-410.
5. Hadrian, R.; Palmes, D., Animal Models of Secondary Lymphedema: New Approaches in the Search for Therapeutic Options. *Lymphat Res Biol* **2017,** *15* (1), 2-16.
6. Shin, W. S.; Rockson, S. G., Animal models for the molecular and mechanistic study of lymphatic biology and disease. *Annals of the New York Academy of Sciences* **2008,** *1131* (1), 50-74.
7. Sato, M.; Sasaki, N.; Ato, M.; Hirakawa, S.; Sato, K.; Sato, K., Microcirculation-on-a-chip: A microfluidic platform for assaying blood-and lymphatic-vessel permeability. *PloS one* **2015,** *10* (9), e0137301.
8. Price, G. M.; Chrobak, K. M.; Tien, J., Effect of cyclic AMP on barrier function of human lymphatic microvascular tubes. *Microvascular research* **2008,** *76* (1), 46-51.
9. Thompson, R. L.; Margolis, E. A.; Ryan, T. J.; Coisman, B. J.; Price, G. M.; Wong, K. H.; Tien, J., Design principles for lymphatic drainage of fluid and solutes from collagen scaffolds. *Journal of Biomedical Materials Research Part A* **2018,** *106* (1), 106-114.
10. Wong, K. H.; Truslow, J. G.; Khankhel, A. H.; Chan, K. L.; Tien, J., Artificial lymphatic drainage systems for vascularized microfluidic scaffolds. *Journal of Biomedical Materials Research Part A* **2013,** *101* (8), 2181-2190.
11. Gong, M. M.; Lugo-Cintron, K. M.; White, B. R.; Kerr, S. C.; Harari, P. M.; Beebe, D. J., Human organotypic lymphatic vessel model elucidates microenvironment-dependent signaling and barrier function. *Biomaterials* **2019,** *214*, 119225.
12. Ayuso, J. M.; Gong, M. M.; Skala, M. C.; Harari, P. M.; Beebe, D. J., Human Tumor‐Lymphatic Microfluidic Model Reveals Differential Conditioning of Lymphatic Vessels by Breast Cancer Cells. *Advanced Healthcare Materials* **2020,** *9* (3), 1900925.
13. Lugo-Cintrón, K. M.; Ayuso, J. M.; White, B. R.; Harari, P. M.; Ponik, S. M.; Beebe, D. J.; Gong, M. M.; Virumbrales-Muñoz, M., Matrix density drives 3D organotypic lymphatic vessel activation in a microfluidic model of the breast tumor microenvironment. *Lab on a Chip* **2020,** *20* (9), 1586-1600.
14. Cao, X.; Ashfaq, R.; Cheng, F.; Maharjan, S.; Li, J.; Ying, G.; Hassan, S.; Xiao, H.; Yue, K.; Zhang, Y. S., A tumor‐on‐a‐chip system with bioprinted blood and lymphatic vessel pair. *Advanced Functional Materials* **2019,** *29* (31), 1807173.
15. Kwak, B.; Ozcelikkale, A.; Shin, C. S.; Park, K.; Han, B., Simulation of complex transport of nanoparticles around a tumor using tumor-microenvironment-on-chip. *Journal of controlled release* **2014,** *194*, 157-167.
16. Pisano, M.; Triacca, V.; Barbee, K.; Swartz, M., An in vitro model of the tumor–lymphatic microenvironment with simultaneous transendothelial and luminal flows reveals mechanisms of flow enhanced invasion. *Integrative biology* **2015,** *7* (5), 525-533.
17. Choi, D.; Park, E.; Jung, E.; Seong, Y. J.; Yoo, J.; Lee, E.; Hong, M.; Lee, S.; Ishida, H.; Burford, J., Laminar flow downregulates Notch activity to promote lymphatic sprouting. *The Journal of clinical investigation* **2017,** *127* (4), 1225-1240.

18. Kim, S.; Chung, M.; Jeon, N. L., Three-dimensional biomimetic model to reconstitute sprouting lymphangiogenesis in vitro. *Biomaterials* **2016,** *78*, 115-128.
19. Arkill, K. P.; Moger, J.; Winlove, C. P., The structure and mechanical properties of collecting lymphatic vessels: an investigation using multimodal nonlinear microscopy. *Journal of anatomy* **2010,** *216* (5), 547-555.
20. von der Weid, P. Y.; Zawieja, D. C., Lymphatic smooth muscle: the motor unit of lymph drainage. *Int J Biochem Cell Biol* **2004,** *36* (7), 1147-53.
21. Kaiser, L.; Mupanomunda, M.; Williams, J. F., Brugia pahangi-induced contractility of bovine mesenteric lymphatics studied in vitro: A role for filarial factors in the development of lymphedema? *The American journal of tropical medicine and hygiene* **1996,** *54* (4), 386-390.
22. Scallan, J. P.; Zawieja, S. D.; Castorena-Gonzalez, J. A.; Davis, M. J., Lymphatic pumping: mechanics, mechanisms and malfunction. *J Physiol* **2016,** *594* (20), 5749-5768.
23. Castorena-Gonzalez, J. A.; Zawieja, S. D.; Li, M.; Srinivasan, R. S.; Simon, A. M.; de Wit, C.; de la Torre, R.; Martinez-Lemus, L. A.; Hennig, G. W.; Davis, M. J., Mechanisms of connexin-related lymphedema: a critical role for Cx45, but not Cx43 or Cx47, in the entrainment of spontaneous lymphatic contractions. *Circulation research* **2018,** *123* (8), 964-985.
24. Hooks, J. S.; Clement, C. C.; Nguyen, H. D.; Santambrogio, L.; Dixon, J. B., In vitro model reveals a role for mechanical stretch in the remodeling response of lymphatic muscle cells. *Microcirculation* **2019,** *26* (1), e12512.
25. Razavi, M. S.; Leonard-Duke, J.; Hardie, B.; Dixon, J. B.; Gleason, R. L., Axial stretch regulates rat tail collecting lymphatic vessel contractions. *Scientific Reports* **2020,** *10* (1), 1-11.
26. Ohtani, Y.; OHTANI, O., Postnatal development of lymphatic vessels and their smooth muscle cells in the rat diaphragm: a confocal microscopic study. *Archives of histology and cytology* **2001,** *64* (5), 513-522.
27. Bridenbaugh, E. A.; Nizamutdinova, I. T.; Jupiter, D.; Nagai, T.; Thangaswamy, S.; Chatterjee, V.; Gashev, A. A., Lymphatic muscle cells in rat mesenteric lymphatic vessels of various ages. *Lymphatic research and biology* **2013,** *11* (1), 35-42.
28. Bischel, L. L.; Lee, S. H.; Beebe, D. J., A practical method for patterning lumens through ECM hydrogels via viscous finger patterning. *J Lab Autom* **2012,** *17* (2), 96-103.
29. de Graaf, M. N.; Cochrane, A.; van den Hil, F. E.; Buijsman, W.; van der Meer, A. D.; van den Berg, A.; Mummery, C. L.; Orlova, V. V., Scalable microphysiological system to model three-dimensional blood vessels. *APL bioengineering* **2019,** *3* (2), 026105.
30. Herland, A.; van der Meer, A. D.; FitzGerald, E. A.; Park, T. E.; Sleeboom, J. J.; Ingber, D. E., Distinct Contributions of Astrocytes and Pericytes to Neuroinflammation Identified in a 3D Human Blood-Brain Barrier on a Chip. *PLoS One* **2016,** *11* (3), e0150360.
31. Jiménez‐Torres, J. A.; Peery, S. L.; Sung, K. E.; Beebe, D. J., LumeNEXT: a practical method to pattern luminal structures in ECM gels. *Advanced healthcare materials* **2016,** *5* (2), 198-204.
32. Lutter, S.; Xie, S.; Tatin, F.; Makinen, T., Smooth muscle–endothelial cell communication activates Reelin signaling and regulates lymphatic vessel formation. *J Cell Biol* **2012,** *197* (6), 837-849.
33. Behringer, E. J.; Scallan, J. P.; Jafarnejad, M.; Castorena‐Gonzalez, J. A.; Zawieja, S. D.; Moore, J. E.; Davis, M. J.; Segal, S. S., Calcium and electrical dynamics in lymphatic endothelium. *The Journal of physiology* **2017,** *595* (24), 7347-7368.
34. Michalaki, E.; Surya, V. N.; Fuller, G. G.; Dunn, A. R., Perpendicular alignment of lymphatic endothelial cells in response to spatial gradients in wall shear stress. *Communications biology* **2020,** *3* (1), 1-9.

35. Andrique, L.; Recher, G.; Alessandri, K.; Pujol, N.; Feyeux, M.; Bon, P.; Cognet, L.; Nassoy, P.; Bikfalvi, A., A model of guided cell self-organization for rapid and spontaneous formation of functional vessels. *Science advances* **2019,** *5* (6), eaau6562.
36. Lee, H.; Kim, S.; Chung, M.; Kim, J. H.; Jeon, N. L., A bioengineered array of 3D microvessels for vascular permeability assay. *Microvascular research* **2014,** *91*, 90-98.
37. Polacheck, W. J.; Kutys, M. L.; Yang, J.; Eyckmans, J.; Wu, Y.; Vasavada, H.; Hirschi, K. K.; Chen, C. S., A non-canonical Notch complex regulates adherens junctions and vascular barrier function. *Nature* **2017,** *552* (7684), 258-262.
38. Song, J. W.; Munn, L. L., Fluid forces control endothelial sprouting. *Proceedings of the National Academy of Sciences* **2011,** *108* (37), 15342-15347.
39. Nguyen, D.-H. T.; Stapleton, S. C.; Yang, M. T.; Cha, S. S.; Choi, C. K.; Galie, P. A.; Chen, C. S., Biomimetic model to reconstitute angiogenic sprouting morphogenesis in vitro. *Proceedings of the National Academy of Sciences* **2013,** *110* (17), 6712-6717.
40. Mandrycky, C.; Hadland, B.; Zheng, Y., 3D curvature-instructed endothelial flow response and tissue vascularization. *Science advances* **2020,** *6* (38), eabb3629.
41. Rayner, S. G.; Phong, K. T.; Xue, J.; Lih, D.; Shankland, S. J.; Kelly, E. J.; Himmelfarb, J.; Zheng, Y., Reconstructing the human renal vascular–tubular unit in vitro. *Advanced healthcare materials* **2018,** *7* (23), 1801120.
42. Heintz, K. A.; Bregenzer, M. E.; Mantle, J. L.; Lee, K. H.; West, J. L.; Slater, J. H., Fabrication of 3D biomimetic microfluidic networks in hydrogels. *Advanced healthcare materials* **2016,** *5* (17), 2153-2160.
43. Menon, N. V.; Su, C.; Pang, K. T.; Phua, Z. J.; Tay, H. M.; Dalan, R.; Wang, X.; Li, K. H. H.; Hou, H. W., Recapitulating atherogenic flow disturbances and vascular inflammation in a perfusable 3D stenosis model. *Biofabrication* **2020,** *12* (4), 045009.
44. Chin, J., Lattice Boltzmann simulation of the flow of binary immiscible fluids with different viscosities using the Shan-Chen microscopic interaction model. *Philosophical Transactions of the Royal Society of London. Series A: Mathematical, Physical and Engineering Sciences* **2002,** *360* (1792), 547-558.
45. Bischel, L. L.; Young, E. W.; Mader, B. R.; Beebe, D. J., Tubeless microfluidic angiogenesis assay with three-dimensional endothelial-lined microvessels. *Biomaterials* **2013,** *34* (5), 1471-1477.
46. Rusznyák, I.; Földi, M.; Szabó, G., *Lymphatics and lymph circulation: physiology and pathology*. Elsevier: 2013.
47. Gaengel, K.; Genové, G.; Armulik, A.; Betsholtz, C., Endothelial-mural cell signaling in vascular development and angiogenesis. *Arteriosclerosis, thrombosis, and vascular biology* **2009,** *29* (5), 630-638.
48. Lavender, M. D.; Pang, Z.; Wallace, C. S.; Niklason, L. E.; Truskey, G. A., A system for the direct co-culture of endothelium on smooth muscle cells. *Biomaterials* **2005,** *26* (22), 4642-4653.
49. Yoshida, H.; Nakamura, M.; Makita, S.; Hiramori, K., Paracrine effect of human vascular endothelial cells on human vascular smooth muscle cell proliferation: transmembrane co-culture method. *Heart and vessels* **1996,** *11* (5), 229-233.
50. Campbell, J. H.; Campbell, G. R., Endothelial cell influences on vascular smooth muscle phenotype. *Annual review of Physiology* **1986,** *48* (1), 295-306.
51. Moore Jr, J. E.; Bertram, C. D., Lymphatic System Flows. *Annual Review of Fluid Mechanics* **2018,** *50* (1).
52. Von Der Weid, P. Y., Lymphatic vessel pumping and inflammation—the role of spontaneous constrictions and underlying electrical pacemaker potentials. *Alimentary pharmacology & therapeutics* **2001,** *15* (8), 1115-1129.

53. Ohhashi, T.; Azuma, T.; Sakaguchi, M., Active and passive mechanical characteristics of bovine mesenteric lymphatics. *American Journal of Physiology-Heart and Circulatory Physiology* **1980,** *239* (1), H88-H95.
54. Choi, D.; Park, E.; Jung, E.; Seong, Y. J.; Hong, M.; Lee, S.; Burford, J.; Gyarmati, G.; Peti-Peterdi, J.; Srikanth, S., ORAI1 activates proliferation of lymphatic endothelial cells in response to laminar flow through Krüppel-like factors 2 and 4. *Circulation research* **2017,** *120* (9), 1426-1439.
55. Dixon, J. B.; Greiner, S. T.; Gashev, A. A.; Cote, G. L.; Moore, J. E.; Zawieja, D. C., Lymph flow, shear stress, and lymphocyte velocity in rat mesenteric prenodal lymphatics. *Microcirculation (New York, N.Y. : 1994)* **2006,** *13* (7), 597-610.
56. Osaki, T.; Kakegawa, T.; Kageyama, T.; Enomoto, J.; Nittami, T.; Fukuda, J., Acceleration of vascular sprouting from fabricated perfusable vascular-like structures. *PloS one* **2015,** *10* (4), e0123735.
57. Park, Y.-G.; Choi, J.; Jung, H.-K.; Song, I. K.; Shin, Y.; Park, S.-Y.; Seol, J.-W., Fluid shear stress regulates vascular remodeling via VEGFR-3 activation, although independently of its ligand, VEGF-C, in the uterus during pregnancy. *International Journal of Molecular Medicine* **2017,** *40* (4), 1210-1216.
58. Yang, Y.; Cha, B.; Motawe, Z. Y.; Srinivasan, R. S.; Scallan, J. P., VE-cadherin is required for lymphatic valve formation and maintenance. *Cell reports* **2019,** *28* (9), 2397-2412. e4.
59. Mortimer, P. S., The pathophysiology of lymphedema. *Cancer: Interdisciplinary International Journal of the American Cancer Society* **1998,** *83* (S12B), 2798-2802.
60. Stanton, A.; Mellor, R.; Cook, G.; Svensson, W.; Peters, A.; Levick, J.; Mortimer, P., Impairment of lymph drainage in subfascial compartment of forearm in breast cancer-related lymphedema. *Lymphatic research and biology* **2003,** *1* (2), 121-132.
61. Zhang, C., The role of inflammatory cytokines in endothelial dysfunction. *Basic research in cardiology* **2008,** *103* (5), 398-406.
62. Chen, Y. The Effects of Pro-Inflammatory Cytokine TNF-α on Rat Mesenteric Lymphatic Pumping and Its Signaling Pathway. Graduate Studies, 2014.
63. Cromer, W. E.; Zawieja, S. D.; Tharakan, B.; Childs, E. W.; Newell, M. K.; Zawieja, D. C., The effects of inflammatory cytokines on lymphatic endothelial barrier function. *Angiogenesis* **2014,** *17* (2), 395-406.
64. Natarajan, R.; Northrop, N.; Yamamoto, B., Fluorescein Isothiocyanate (FITC)‐Dextran Extravasation as a Measure of Blood‐Brain Barrier Permeability. *Current protocols in neuroscience* **2017,** *79* (1), 9.58. 1-9.58. 15.
65. Ono, N.; Mizuno, R.; Ohhashi, T., Effective permeability of hydrophilic substances through walls of lymph vessels: roles of endothelial barrier. *American Journal of Physiology-Heart and Circulatory Physiology* **2005,** *289* (4), H1676-H1682.
66. Zawieja, D. C., Lymphatic microcirculation. *Microcirculation* **1996,** *3* (2), 241-3.
67. Gashev, A. A., Lymphatic vessels: pressure- and flow-dependent regulatory reactions. *Ann N Y Acad Sci* **2008,** *1131*, 100-9.
68. Saharinen, P.; Tammela, T.; Karkkainen, M. J.; Alitalo, K., Lymphatic vasculature: development, molecular regulation and role in tumor metastasis and inflammation. *Trends in immunology* **2004,** *25* (7), 387-395.
69. Margaris, K. N.; Black, R. A., Modelling the lymphatic system: challenges and opportunities. *J R Soc Interface* **2012,** *9* (69), 601-12.
70. Gold, K.; Gaharwar, A. K.; Jain, A., Emerging trends in multiscale modeling of vascular pathophysiology: Organ-on-a-chip and 3D printing. *Biomaterials* **2018**.
71. Su, C.; Menon, N. V.; Xu, X.; Teo, Y. R.; Cao, H.; Dalan, R.; Tay, C. Y.; Hou, H. W., A novel human arterial wall-on-a-chip to study endothelial inflammation and vascular smooth muscle cell migration in early atherosclerosis. *Lab on a Chip* **2021**.

72. Humayun, M.; Chow, C.-W.; Young, E. W., Microfluidic lung airway-on-a-chip with arrayable suspended gels for studying epithelial and smooth muscle cell interactions. *Lab on a Chip* **2018,** *18* (9), 1298-1309.
73. Deng, X.; Marinov, G.; Marois, Y.; Guidoin, R., Mechanical characteristics of the canine thoracic duct: what are the driving forces of the lymph flow? *Biorheology* **1999,** *36* (5, 6), 391-399.
74. MacDonald, A. J.; Arkill, K. P.; Tabor, G. R.; McHale, N. G.; Winlove, C. P., Modeling flow in collecting lymphatic vessels: one-dimensional flow through a series of contractile elements. *American Journal of Physiology-Heart and Circulatory Physiology* **2008,** *295* (1), H305-H313.
75. Andrae, J.; Gallini, R.; Betsholtz, C., Role of platelet-derived growth factors in physiology and medicine. *Genes & development* **2008,** *22* (10), 1276-1312.
76. Donovan, J.; Abraham, D.; Norman, J., Platelet-derived growth factor signaling in mesenchymal cells. *Front Biosci (Landmark Ed)* **2013,** *18* (1), 106-119.
77. Ziegler, T.; Alexander, R. W.; Nerem, R. M., An endothelial cell-smooth muscle cell co-culture model for use in the investigation of flow effects on vascular biology. *Ann Biomed Eng* **1995,** *23* (3), 216-25.
78. Schwager, S.; Detmar, M., Inflammation and lymphatic function. *Frontiers in immunology* **2019,** *10*, 308.
79. Scallan, J. P.; Huxley, V. H., In vivo determination of collecting lymphatic vessel permeability to albumin: a role for lymphatics in exchange. *The Journal of physiology* **2010,** *588* (1), 243-254.
80. Jannaway, M.; Scallan, J. P., VE-Cadherin and Vesicles Differentially Regulate Lymphatic Vascular Permeability to Solutes of Various Sizes. *Frontiers in Physiology* **2021,** *12*.
81. Gashev, A. A.; Davis, M. J.; Gasheva, O. Y.; Nepiushchikh, Z. V.; Wang, W.; Dougherty, P.; Kelly, K. A.; Cai, S.; Von Der Weid, P.-Y.; Muthuchamy, M., Methods for lymphatic vessel culture and gene transfection. *Microcirculation* **2009,** *16* (7), 615-628.
82. Akl, T. J.; Coté, G. L.; Nepiyushchikh, Z. V.; Gashev, A. A.; Zawieja, D. C., Measuring contraction propagation and localizing pacemaker cells using high speed video microscopy. *Journal of biomedical optics* **2011,** *16* (2), 026016.
83. Hald, B. O.; Castorena-Gonzalez, J. A.; Zawieja, S. D.; Gui, P.; Davis, M. J., Electrical communication in lymphangions. *Biophysical journal* **2018,** *115* (5), 936-949.
84. Al‐Kofahi, M.; Becker, F.; Gavins, F.; Woolard, M.; Tsunoda, I.; Wang, Y.; Ostanin, D.; Zawieja, D.; Muthuchamy, M.; von der Weid, P., IL‐1β reduces tonic contraction of mesenteric lymphatic muscle cells, with the involvement of cycloxygenase‐2 and prostaglandin E 2. *British journal of pharmacology* **2015,** *172* (16), 4038-4051.
85. Jain, A.; Mathur, T.; Pandian, N. K.; Selahi, A., Organ-on-a-chip and 3D printing as preclinical models for medical research and practice. In *Precision Medicine for Investigators, Practitioners and Providers*, Elsevier: 2020; pp 83-95.
86. Kim, D.; Herr, A. E., Protein immobilization techniques for microfluidic assays. *Biomicrofluidics* **2013,** *7* (4), 041501.
87. Hayes, H.; Kossmann, E.; Wilson, E.; Meininger, C.; Zawieja, D., Development and characterization of endothelial cells from rat microlymphatics. *Lymphatic research and biology* **2003,** *1* (2), 101-119.
88. Muthuchamy, M.; Gashev, A.; Boswell, N.; Dawson, N.; Zawieja, D., Molecular and functional analyses of the contractile apparatus in lymphatic muscle. *FASEB J* **2003,** *17* (8), 920-2.
89. Zhang, X.; Chakraborty, S.; Muthuchamy, M.; Zawieja, D. C., Isolation of Lymphatic Muscle Cells (LMCsLymphatic muscle cells (LMCs)) from Rat Mesentery. In

Cardiovascular Development: Methods and Protocols, Peng, X.; Zimmer, W. E., Eds. Springer US: New York, NY, 2021; pp 137-141.
90. Voyta, J. C.; Via, D. P.; Butterfield, C. E.; Zetter, B. R., Identification and isolation of endothelial cells based on their increased uptake of acetylated-low density lipoprotein. *Journal of Cell Biology* **1984,** *99* (6), 2034-2040.
91. Mathur, T.; Singh, K. A.; Pandian, N. K.; Tsai, S.-H.; Hein, T. W.; Gaharwar, A. K.; Flanagan, J. M.; Jain, A., Organ-on-chips made of blood: endothelial progenitor cells from blood reconstitute vascular thromboinflammation in vessel-chips. *Lab on a Chip* **2019,** *19* (15), 2500-2511.
92. Akl, T. J.; Nagai, T.; Coté, G. L.; Gashev, A. A., Mesenteric lymph flow in adult and aged rats. *American Journal of Physiology-Heart and Circulatory Physiology* **2011,** *301* (5), H1828-H1840.
93. Busschots, S.; O'Toole, S.; O'Leary, J. J.; Stordal, B., Non-invasive and non-destructive measurements of confluence in cultured adherent cell lines. *MethodsX* **2015,** *2*, 8-13.
94. Schindelin, J.; Arganda-Carreras, I.; Frise, E.; Kaynig, V.; Longair, M.; Pietzsch, T.; Preibisch, S.; Rueden, C.; Saalfeld, S.; Schmid, B., Fiji: an open-source platform for biological-image analysis. *Nature methods* **2012,** *9* (7), 676-682.
95. Püspöki, Z.; Storath, M.; Sage, D.; Unser, M., Transforms and operators for directional bioimage analysis: a survey. In *Focus on Bio-Image Informatics*, Springer: 2016; pp 69-93.
96. Rezakhaniha, R.; Agianniotis, A.; Schrauwen, J. T. C.; Griffa, A.; Sage, D.; Bouten, C. v.; Van De Vosse, F.; Unser, M.; Stergiopulos, N., Experimental investigation of collagen waviness and orientation in the arterial adventitia using confocal laser scanning microscopy. *Biomechanics and modeling in mechanobiology* **2012,** *11* (3-4), 461-473.
97. Chaitanya, G.; Franks, S.; Cromer, W.; Wells, S.; Bienkowska, M.; Jennings, M.; Ruddell, A.; Ando, T.; Wang, Y.; Gu, Y., Differential cytokine responses in human and mouse lymphatic endothelial cells to cytokines in vitro. *Lymphatic research and biology* **2010,** *8* (3), 155-164.
98. Bove, K.; Neumann, P.; Gertzberg, N.; Johnson, A., Role of ecNOS-derived NO in mediating TNF-induced endothelial barrier dysfunction. *American Journal of Physiology-Lung Cellular and Molecular Physiology* **2001,** *280* (5), L914-L922.
99. Huxley, V.; Curry, F.; Adamson, R., Quantitative fluorescence microscopy on single capillaries: alpha-lactalbumin transport. *American Journal of Physiology-Heart and Circulatory Physiology* **1987,** *252* (1), H188-H197.

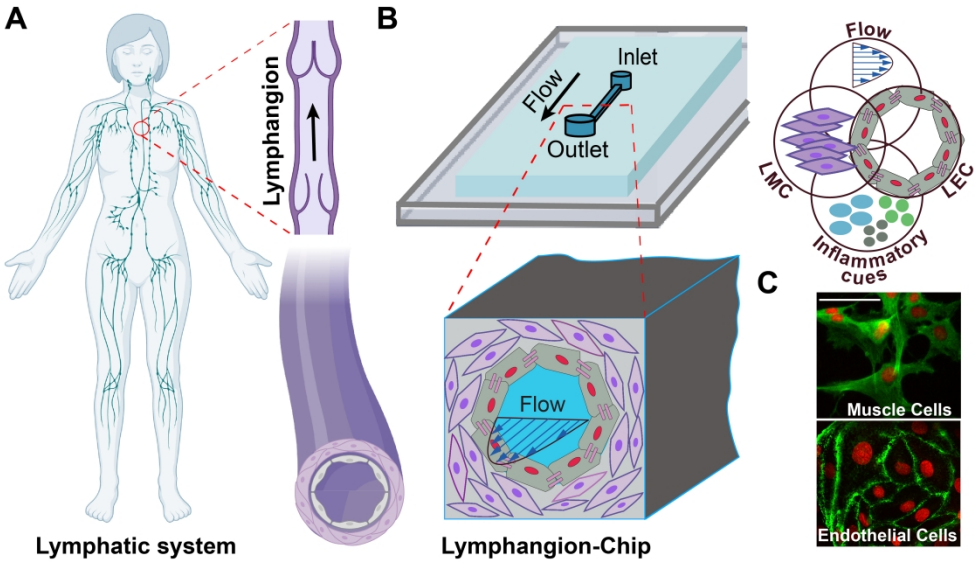

1

464x281mm (236 x 236 DPI)

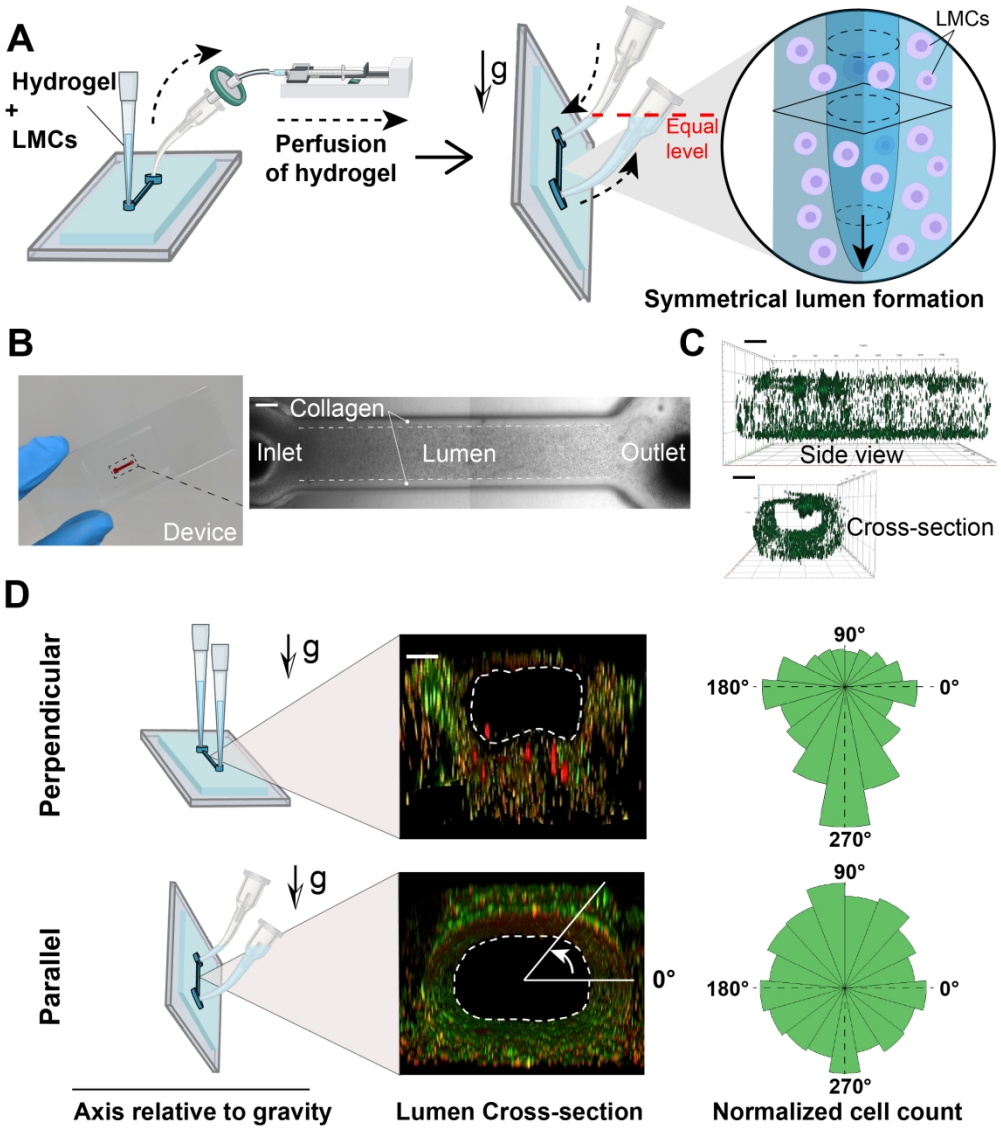

2

259x291mm (236 x 236 DPI)

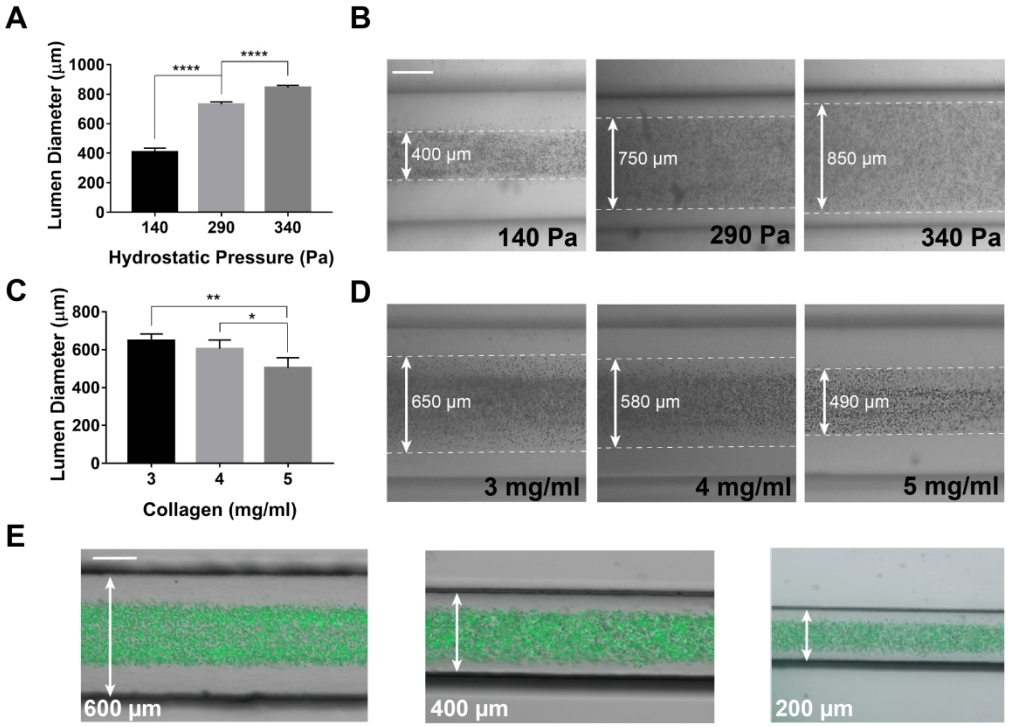

3

351x254mm (236 x 236 DPI)

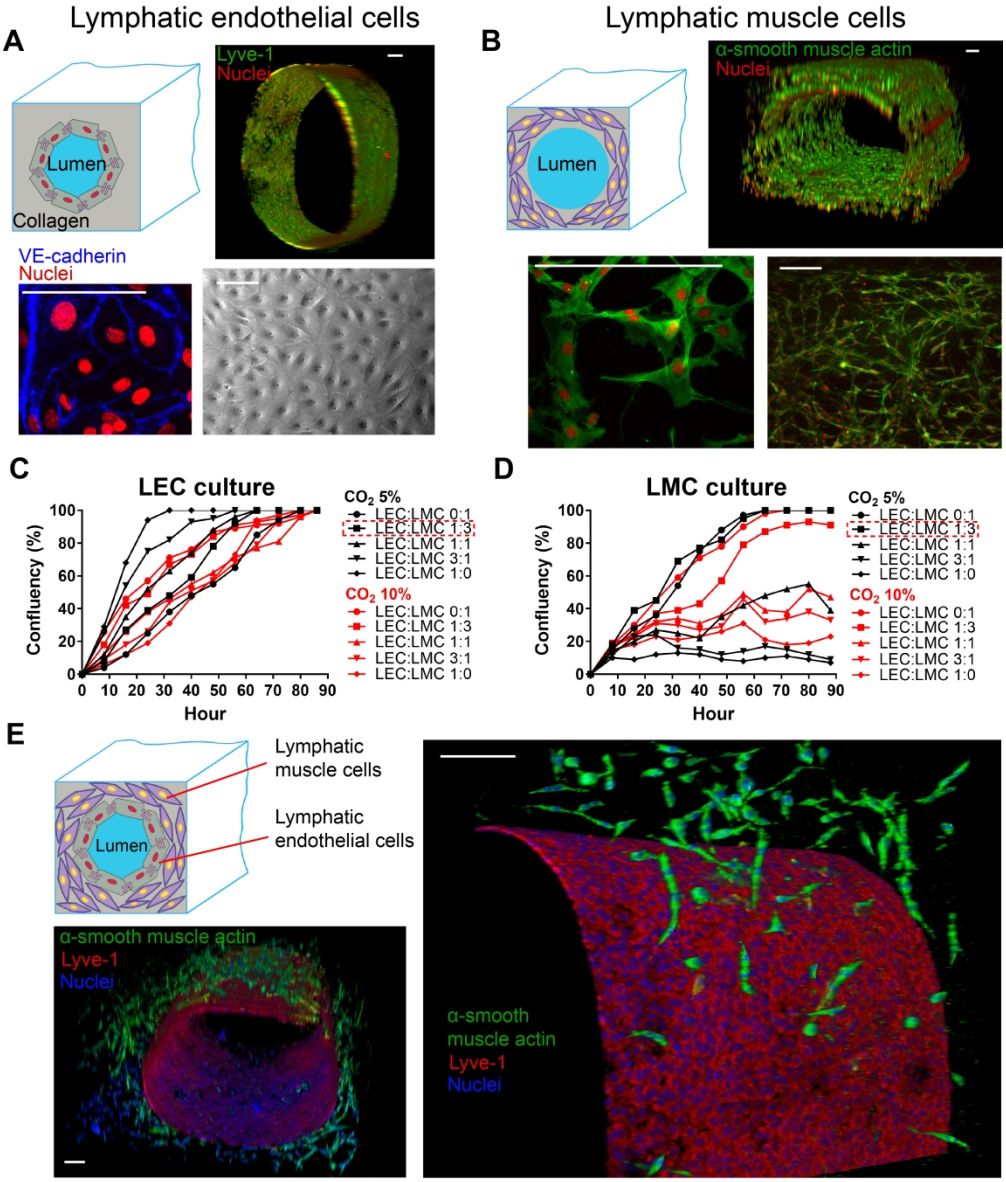

4

366x430mm (236 x 236 DPI)

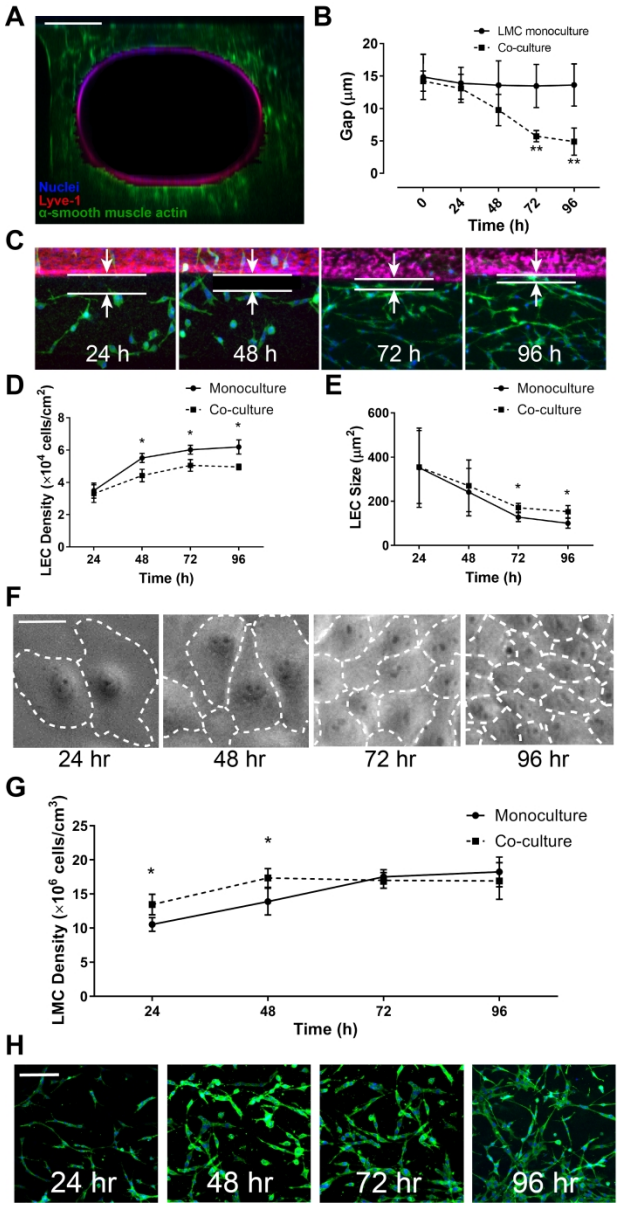

5

241x471mm (236 x 236 DPI)

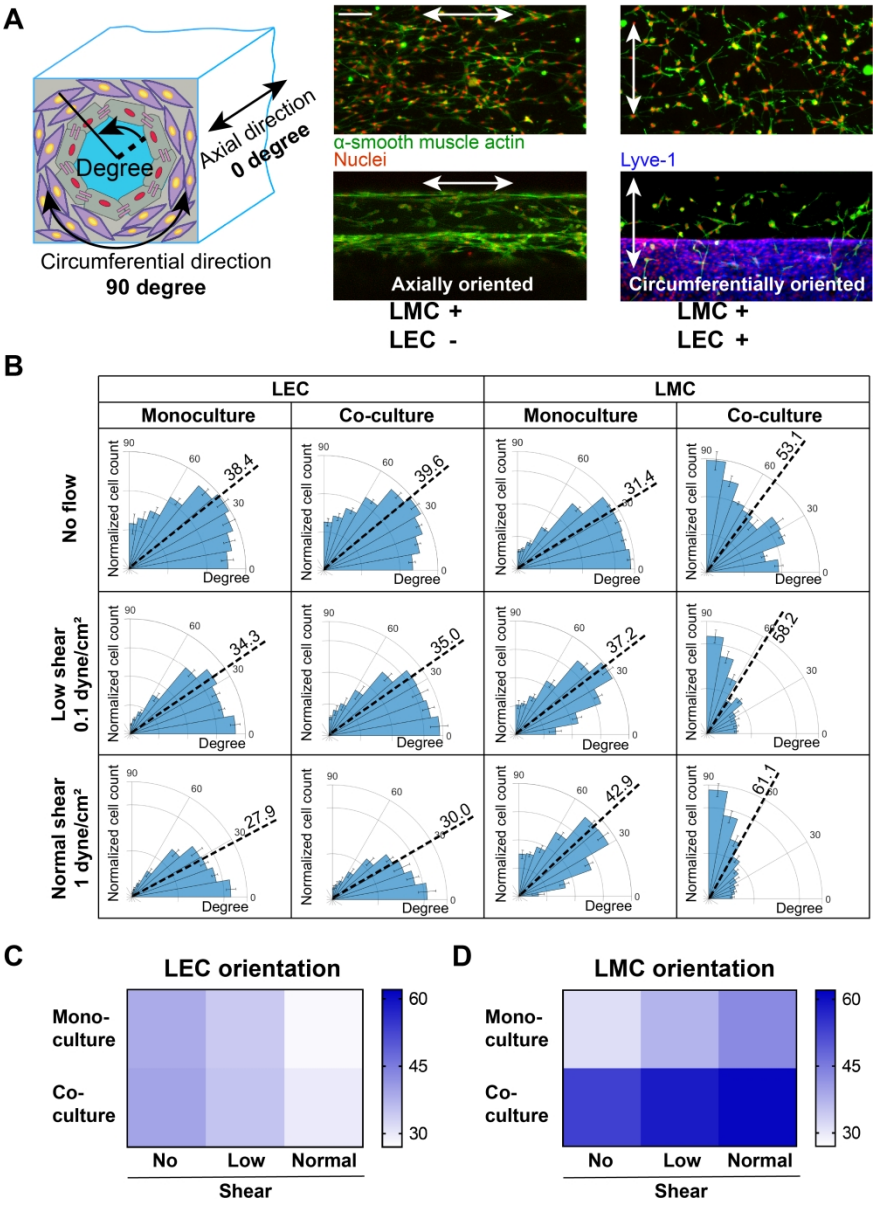

6

327x450mm (236 x 236 DPI)

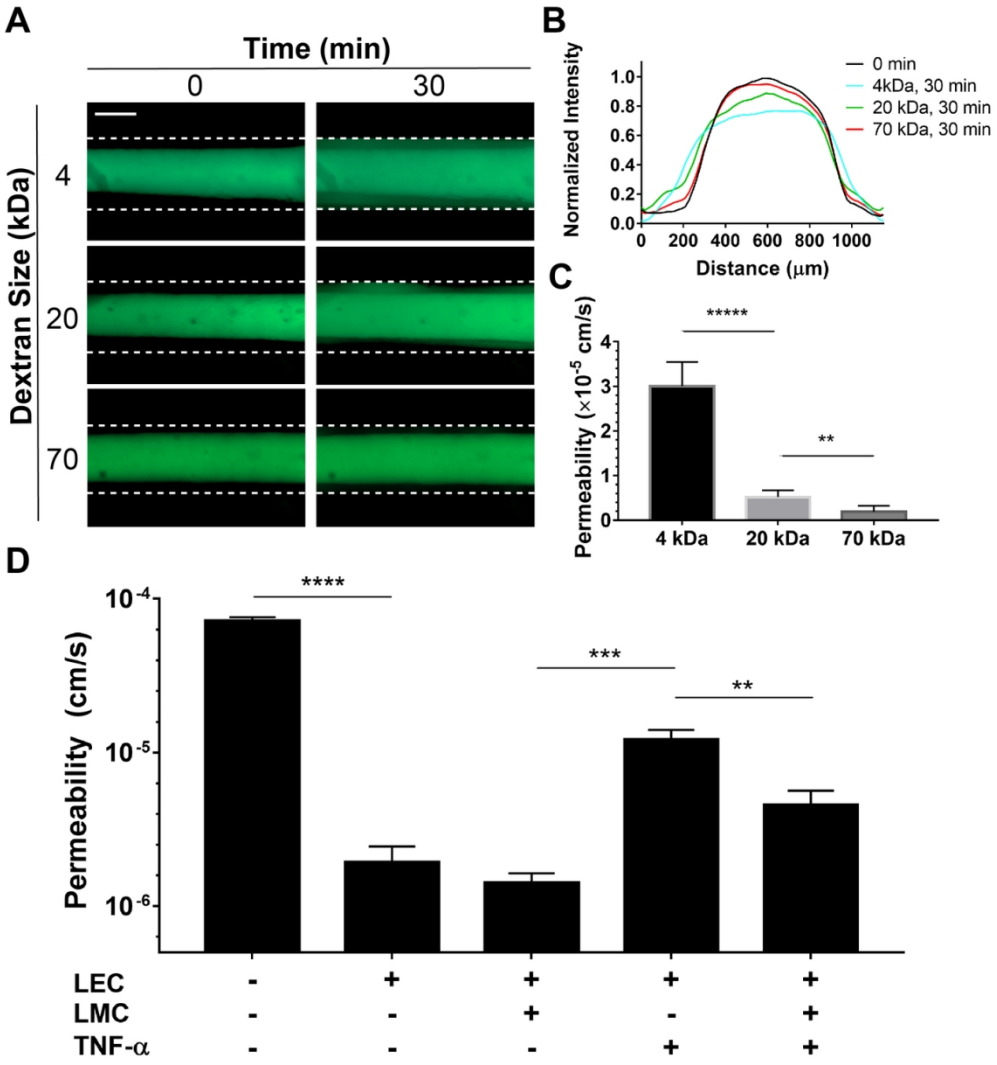

7

119x132mm (300 x 300 DPI)